© 2017. Published by The Company of Biologists Ltd | Journal of Cell Science (2017) 130, 490-501 doi:10.1242/jcs.193821

RESEARCH ARTICLE

Phosphorylation of filamin A regulates chemokine receptor CCR2 recycling

Mònica Pons[1,¶], Ismael Izquierdo[1,¶], Mireia Andreu-Carbó[1], Georgina Garrido[1,*], Jesús Planagumà[2,‡], Olivia Muriel[3,§], Miguel A. del Pozo[3], M. Isabel Geli[1] and Anna M. Aragay[1,]**

ABSTRACT

Proper endosomal trafficking of ligand-activated G-protein-coupled receptors (GPCRs) is essential to spatiotemporally tune their physiological responses. For the monocyte chemoattractant receptor 2 (CCR2B; one of two isoforms encoded by *CCR2*), endocytic recycling is important to sustain monocyte migration, whereas filamin A (FLNa) is essential for CCL2-induced monocyte migration. Here, we analyze the role of FLNa in the trafficking of CCR2B along the endocytic pathway. In FLNa-knockdown cells, activated CCR2B accumulated in enlarged EEA-1-positive endosomes, which exhibited slow movement and fast fluorescence recovery, suggesting an imbalance between receptor entry and exit rates. Utilizing super-resolution microscopy, we observed that FLNa–GFP, CCR2B and β2-adrenergic receptor (β2AR) were present in actin-enriched endosomal microdomains. Depletion of FLNa decreased CCR2B association with these microdomains and concomitantly delayed CCR2B endosomal traffic, without apparently affecting the number of microdomains. Interestingly, CCR2B and β2AR signaling induced phosphorylation of FLNa at residue S2152, and this phosphorylation event was contributes to sustain receptor recycling. Thus, our data strongly suggest that CCR2B and β2AR signals to FLNa to stimulate its endocytosis and recycling to the plasma membrane.

KEY WORDS: GPCR, CCR2, Filamin A, Recycling

INTRODUCTION

A key aspect of the cellular responses mediated by G-protein-coupled receptors (GPCRs) is the spatiotemporal regulation of their signaling, which occurs at the level of ligand binding but also through control of the number of receptors on the cell surface. Therefore, explaining the control of receptor sorting into different degradative or recycling endocytic pathways is fundamental to understand GPCR function. Once internalized, receptors follow different fates inside the cell: some rapidly return to the plasma membrane from the sorting endosome, others travel to the perinuclear endosomes for slower recycling or are transported to lysosomes for degradation. Receptor sorting within endosome trafficking is facilitated by dynamic actin filaments, which are generated through WASH and the Arp 2/3 complex at the surface of endosomes (Derivery et al., 2009; Gomez and Billadeau, 2009) and specialized protein interactions. Some GPCRs, such as β2-adrenergic receptor (β2AR), have specific sequences that trap the receptor in endosomal actin-enriched subdomains for transport along the short recycling route – so called 'sequence-dependent' recycling (Cao et al., 1999; Puthenveedu et al., 2010). The sequence-dependent pathways require PDZ-containing proteins and the retromer complex (Temkin et al., 2011). In those routes, the actin-enriched subdomains are thought to function as platforms that capture cargo proteins into retromer tubules, retrieving them from the default pathway.

The diversity of actin functions along the endocytic pathway is the result of proteins that precisely control the architecture of the actin networks and of the interacting partners among the endocytic cargo and the endocytic machinery. Some of the most prominent actin-cross-linking proteins in higher eukaryotes are the filamins (filamin A, B and C; FLNa, FLNb and FLNc, respectively) (Nakamura et al., 2011). FLNa is a dimeric protein with 24 immunoglobulin (Ig) repeats that cross-link rod-like actin filaments at right angles, creating three-dimensional networks (Hartwig et al., 1980). FLNa exists as an autoinhibitory form that involves Ig repeat 20 (Lad et al., 2007). In addition, FLNa binds to a myriad of cellular proteins of great functional diversity, acting as a scaffold and facilitating protein–protein interactions (Popowicz et al., 2006). Thereby, FLNa integrates the cellular architecture and signaling cascades that are essential for fetal development and cell locomotion. Not surprisingly, mutations in FLNa are linked to a large number of developmental diseases (Savoy and Ghosh, 2013). Among its partners are several GPCRs (Awata et al., 2001; Kim et al., 2005; Onoprishvili et al., 2003; Yu et al., 2008), including several chemokine receptors: CCR2B (one of two alternative splice forms encoded by *CCR2*) (Minsaas et al., 2010; Planagumà et al., 2012), CCR5 and CXCR4 (Gómez-Moutón et al., 2015; Jiménez-Baranda et al., 2007). The exact role of FLNa binding to chemokine receptors is not well understood yet, but much work indicates its function in endocytic traffic and receptor internalization (Cho et al., 2007; Kim et al., 2005; Onoprishvili et al., 2003; Seck et al., 2003). Moreover, FLNa binds to β-arrestin-2, a well-defined GPCR adaptor for clathrin-mediated internalization (Kim et al., 2005; Scott et al., 2006). Recently, FLNa has been suggested to cooperate with binding of β-arrestin-2 to the CXCR4 receptor carrying mutations in arginine residue 334 that are present in WHIM syndrome, which could have implications in WHIM-mutant CXCR4 signaling (Gómez-Moutón et al., 2015).

We have previously shown that FLNa, through predominantly Ig repeats 19–23, binds to the C-terminal tail of the monocyte chemoattractant receptor 2 (CCR2, isoform B) (Minsaas et al., 2010). CCR2 and its ligand, the monocyte chemoattractant protein 1

[1]Department of Biology, Molecular Biology Institute of Barcelona (IBMB), Spanish National Research Council (CSIC), Barcelona 08028, Spain. [2]Department of Biomedicine, University of Bergen, Bergen, 5009 Norway. [3]Centro Nacional de Investigaciones Cardiovasculares, Madrid 28029, Spain.
*Present address: Centre for Genomic Regulation (CRG), Barcelona 08003, Spain.
‡Present address: Department of Neuroimmunology, IDIBAPS, Barcelona, Spain.
§Present address: Department of Fundamental Microbiology, University of Lausanne, Quartier UNIL-Sorge, Bâtiment Biophore 1015 Lausanne, Switzerland.
¶These authors contributed equally to this work

**Author for correspondence (aarbmc@ibmb.csic.es)

Received 15 June 2016; Accepted 18 November 2016

Journal of Cell Science

Journal of Cell Science (2017) 130, 490-501 doi:10.1242/jcs.193821

(CCL2), are involved in a wide variety of pathophysiological inflammatory processes (Deshmane et al., 2009; Johnson et al., 2005; Sallusto and Baggiolini, 2008) and neurodegenerative disorders (Bose and Cho, 2013). Similar to most ligand-bound GPCRs, CCL2-stimulated CCR2 is internalized in clathrin-coated vesicles (García Lopez et al., 2009), which is important to regulate its cellular signaling response (García Lopez et al., 2009; Jiménez-Sainz et al., 2003). The interaction of FLNa with the C-terminal region of CCR2B is essential for receptor internalization in endocytic vesicles and for CCL2-induced monocyte migration (Minsaas et al., 2010; Planagumà et al., 2012). Here, we show that FLNa contributes to CCR2B recycling by controlling the motility of endosomes and the entrance of the receptor into the endosomal actin microdomains that recruit cargo destined for the short-loop recycling pathway. We further show that CCL2-induced phosphorylation of FLNa at S2152 is required to facilitate receptor recycling, suggesting that GPCRs can control the membrane-traffic machinery and spatiotemporally tune its signaling. We have also demonstrated that this mechanism is shared by other GPCRs.

RESULTS

CCR2B accumulates in enlarged early endosomes in FLNa-depleted cells

CCR2B directly interacts with the Rod 1 domain of FLNa, within Ig repeat 19, through the C-terminal intracellular domain of the receptor. This interaction facilitates internalization of the ligand-activated receptor into clathrin-coated pits (Minsaas et al., 2010). We noticed that endosomal structures containing CCR2B appeared to be more peripherally distributed upon ligand stimulation in the human melanoma cell line M2 (lacking expression of FLNa) compared with the isogenic cell line (Minsaas et al., 2010). Initial experiments published previously had also indicated a defect in receptor recycling upon FLNa depletion (Minsaas et al., 2010). This suggests that FLNa plays roles in CCR2B endosomal trafficking, other than those previously reported. To analyze the role of FLNa in CCR2B trafficking through the endocytic pathway, the internalization of Flag–CCR2B was followed with live confocal microscopy in HeLa cells that had been depleted of FLNa by utilizing short hairpin (sh)RNAs (Fig. 1A; Fig. S1A). The results were consistent with previous data and showed CCR2B in peripheral endosomal structures in the absence of FLNa, 30 min after addition of CCL2 (Fig. S1B). Close observation of receptor-loaded endosomes by live confocal imaging revealed an apparent enlargement of the CCR2B-loaded organelles in cells that had been treated with two different shRNAs against FLNa (shFLNa28 and shFLNa29) (Fig. 1A; Fig. S1B). Morphometric analysis showed a significant 1.4-fold increase in the diameter of the CCR2B-loaded endosomes ($P<0.001$, one way ANOVA) in the absence of FLNa (Fig. 1B).

To study the nature of the enlarged endosomal particles, HeLa cells that expressed CCR2B were stimulated with CCL2 at different times, fixed and co-labeled with antibodies against Flag and EEA-1 (Fig. 1C; see Fig. S1C for lower magnification). Some internalized CCR2B particles colocalized with EEA-1 in the presence or absence of FLNa 15 min after CCL2 addition, but the localization of internalized CCR2B with EEA1 became more apparent in shFLNa (shFLNa28)- than in control (shScr)-treated cells at later time points (30 min) (Fig. 1C). This suggests that, although the arrival and exit rates of CCR2B from EEA1-positive endosomes reached the steady-state 15 min after addition of CCL2 in control cells, CCR2B continued to accumulate in the absence of FLNa over at least 15 more minutes. Quantification of fluorescence indicated that knockdown of FLNa expression increased the colocalization of CCR2B with EEA-1 endosomes 1.6-fold ($P<0.05$, two way ANOVA) at 30 min, compared to controls (Fig. 1D). This implied that, in the absence of FLNa, the EEA-1-labeled endosomes kept their capacity to receive incoming vesicles from the plasma membrane for at least 30 min after addition of CCL2 and that the exit of CCR2 from early endosomes was delayed.

FLNa contributes to early endosomal motility

As the receptor accumulates in enlarged early endosomes in the absence of FLNa, we studied the effect of FLNa depletion on the dynamic behavior of CCR2B-loaded endosomes using high-speed [20 frames per second (fps)] imaging. Analysis of immunolabeled CCR2B-positive endosome trajectories that lasted more than 1 min showed a reduction in endosomal velocity [25±5% (mean±s.e.m.) slower than that of controls] and distance traveled [30±5.5% (mean±s.e.m.) shorter than that in controls] in shFLNa cells (Fig. 2A). Significant differences were observed within 15 and 30 min after addition of CCL2, which were independent of the size of the endocytic structures. These experiments allowed us to observe long-range endosome trajectories directed towards the perinuclear region in control cells, whereas in shFLNa cells, CCR2B endosomes moved in random directions with their trajectories remaining close to the origin (Fig. 2B).

To analyze the balance between CCR2B entry and exit rates in and out of sorting endosomes, fluorescent resonance after photobleaching (FRAP) experiments were conducted in living cells expressing Rab4A–YFP, loaded with Alexa-Fluor-647-conjugated antibodies against CCR2B. Endosomes with similar levels of CCR2B–Alexa-Fluor-647 fluorescence and size were selected, and one whole endosome was bleached in its entirety. After FRAP, only 11±1.3% (mean±s.e.m.) of the receptor signal on Rab4A-containing endosomes was recovered after 2.5 min in control cells (Fig. 2C, upper panels; Movie 1). The recovery of the CCR2B signal was faster in the shFLNa cells [18±1.8% (mean±s.e.m.) after 2.5 min (Fig. 2D), compared to controls and to bleached Rab4A–YFP, which showed no differences (Fig. S2; Movie 2). This was despite FLNa depletion hindering the internalization of CCR2B and the motility of the primary endocytic vesicles. Taken together, the data strongly suggest that the exit of CCR2B from sorting endosomes was impaired in the absence of FLNa.

FLNa facilitates CCR2B and β2AR loading in actin rich subdomains

To study which route CCR2B follows back to the plasma membrane, we analyzed the extent of its colocalization with Rab4A and compared it with that of other well-known receptors [transferrin (Tfn) receptor, β2AR, PAR1 (also known as F2R) and ETB (also known as EDNRB)] (Fig. 3A,B). CCL2-stimulated CCR2B, as well as the other receptors, accumulated in microdomains along the Rab4A-decorated endosome membrane. Utilizing line fluorescence correlation (Fig. 3A,B), we found that Tfn was present in most Rab4A-labeled microdomains; consistent with previous reports showing the Tfn receptor can follow both the short- and the long-loop recycling routes (Mayle et al., 2012). Other GPCRs (PAR1 and Etb), which are sorted to lysosomes (Shapiro and Coughlin, 1998; Terada et al., 2014), hardly correlated with Rab4A microdomains (Fig. 3B; Fig. S3). In contrast, internalized CCR2B coincided with about 20% of the Rab4A-enriched microdomains, similar to β2AR, which mainly follows the short recycling loop from the sorting endosome to the plasma membrane.

Journal of Cell Science (2017) 130, 490-501 doi:10.1242/jcs.193821

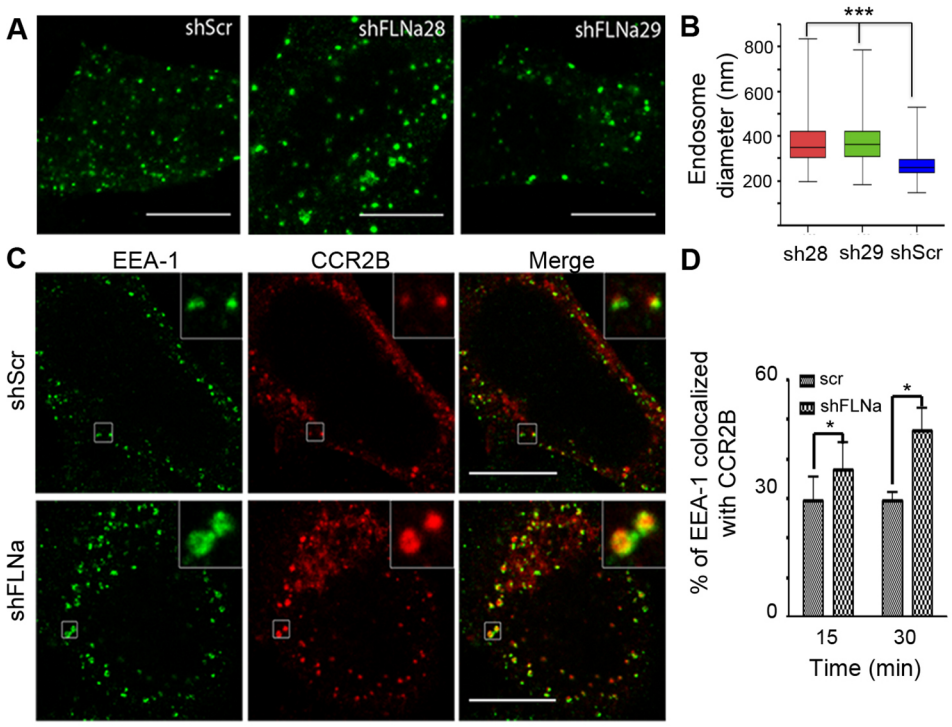

Fig. 1. FLNa knockdown promotes accumulation of CCR2B at early endosomes. (A) Confocal micrographs of live HeLa cells that had been transfected with shRNAs against FLNa (shFLNa28 and shFLNa29, also referred to as sh28 and sh29, respectively) or a scrambled control (shScr) and plated in glass chambers. The cells also expressed Flag–CCR2B, were surface labeled with anti-Flag and Alexa-Fluor-488-conjugated anti-mouse antibodies. Images were captured 60 min after CCL2 addition in a sealed chamber under 5% CO_2 at 37°C. See Fig. S1C for images with low magnification. (B) Box plots showing the endosome diameter measured using the line tool of the software Las Af (Leica microsystems). Lines represent the median, and boxes show the 25th and 75th percentiles of the endosome diameters in sh28, sh29 and shScr cells. Whiskers indicate s.d. A minimum of eight cells in three separate experiments were quantified with 30 endosomes per cell, approximately. Data were analyzed using one way ANOVA test (***P<0.001). (C) Confocal micrographs of HeLa cells expressing shFLNa28 and shScr along with CCR2B, were incubated with 20 nM CCL2 for 15 min at 37°C, fixed and immunostained with anti-EEA-1 antibodies followed by Alexa-Fluor-488-conjugated and M1 anti-Flag antibodies, and then with an Alexa-Fluor-568-conjugated secondary antibody, washed and mounted with ProLong. Magnified images corresponding to small boxes are shown in the insets. Scale bars: 10 µm. See Fig. S1C for a wider-field image. (D) Quantification of the EEA-1 that colocalized with CCR2B in cells treated as described in C, 15 and 30 min after addition of 20 nM CCL2. Significance was determined using one way ANOVA testing of three independent experiments. A significant difference was not found between 15 and 30 min for each shRNA-treated cell line, and there was a significant difference between shScr and shFLNa at each time point (*P<0.05). Imaging was performed with a Leica TCS SP5 using a 63×1.3 NA oil immersion lens. Scale bars: 10 µm.

In fact, CCR2B (Flag–CCR2B) and β2AR (HA–β2AR) often colocalized or were found in close apposition on endosomal microdomains and moved together along the endosomal membrane (Fig. 3C,D), indicating that they follow the same trafficking pathway. As previously described (Temkin et al., 2011), β2AR microdomains were positive for coronin2–GFP, which marks the actin-enriched structures that trap cargo destined for the short-loop recycling pathway from sorting endosomes to the plasma membrane (Fig. 3E, lower panel). Consistent with the view that CCR2B followed the same route as coronin2, CCR2B-labeled microdomains also localized with coronin2–GFP (Fig. 3E, see also line profile).

To investigate if FLNa might be directly involved in the endosomal trafficking of CCR2, super-resolution microscopy (STED) was utilized to determine its presence on endosomes. The fluorescence signal of a functional FLNa–GFP construct (Planagumà et al., 2012) was most apparent at the cortex of HeLa cells (Fig. 4A). However, taking a sagittal plane of the cell, FLNa–GFP could be detected at discrete dynamic subdomains on the surface of vacuolar structures (Fig. 4A, lower panel). Interestingly, FLNa–DsRed colocalized with coronin2–GFP dots on the vacuolar membranes, indicating that FLNa might directly participate in the function and regulation of the actin-enriched microdomains in trapping cargo for the retromer pathway to the plasma membrane (Fig. 4B). To confirm so, we investigated whether some of these FLNa–GFP microdomains coincided with internalized fluorescence-labeled CCR2B. CCR2B was present in Rab4A–Cherry-labeled sorting endosomes in accumulations, which transiently coincided with FLNa–GFP microdomains (Fig. 4C,D; see Movies 3 and 4). The CCR2B- and FLNa-labeled accumulations were very mobile (Fig. 4C). As anticipated, FLNa–GFP localized with actin–RFP and CCR2B on receptor-loaded early endosomes (Fig. 4D). It was also possible to observe FLNa together with CCR2B on domains in Rab5A–Cherry-labeled endosomes (Fig. 4D; Movie 4). However, little coincidence was observed in Rab11–Cherry-labeled endosomes (Fig. 4D; Movie 5). These results indicate that FLNa and CCR2B colocalized on the endosomal actin and coronin2-enriched early endosomal microdomains, similar to internalized HA– β2AR (Fig. 4E, see also Fig. 5).

We next asked if FLNa is important to maintain the actin-enriched endosomal subdomains. Depletion of FLNa did not alter either the number or the intensity of the coronin2–GFP patches on the endosomes (Fig. 5A,B), suggesting that FLNa is not essential to generate or maintain the structure of coronin2–actin patches on endosomes. Strikingly though, we observed that depletion of FLNa clearly decreased the association of fluorescence-labeled

Journal of Cell Science (2017) 130, 490-501 doi:10.1242/jcs.193821

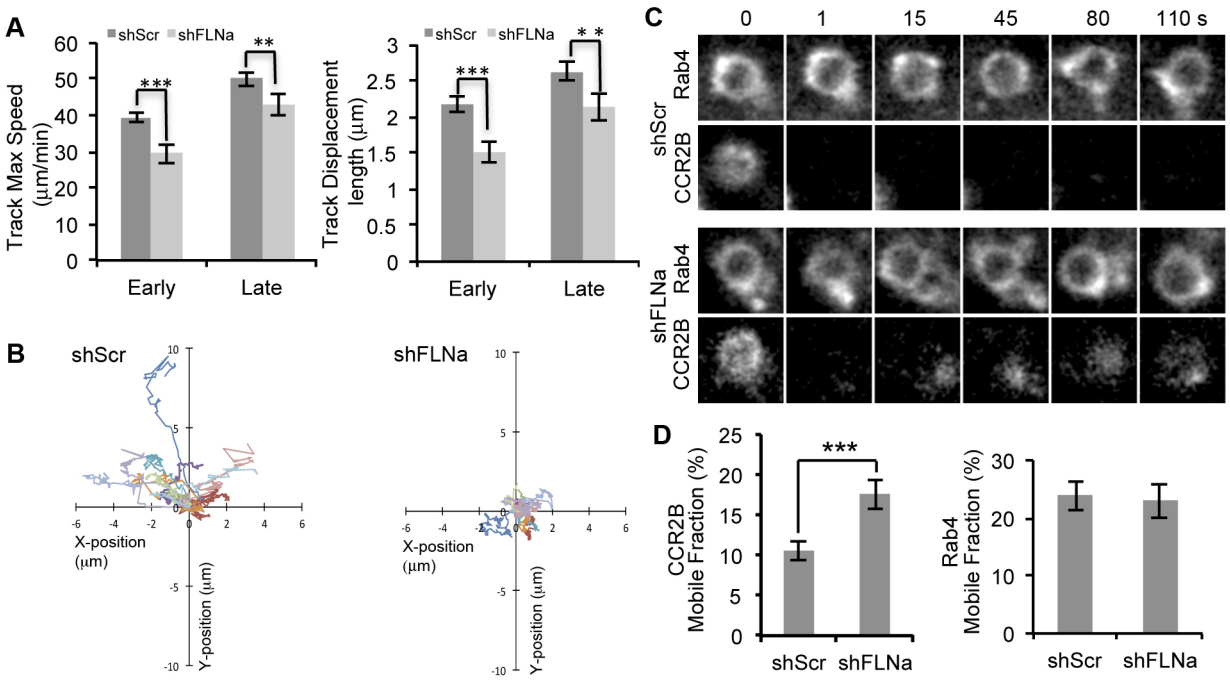

Fig. 2. The motility and fluorescence recovery of endosomes is affected in FLNa-knockdown cells. (A) The track speed (left) and track length (right) of CCR2B-loaded endosomes in shFLNa and shScr HEK293 cells that had been transfected with Flag–CCR2B and surface labeled with anti-Flag and Alexa-Fluor-568-conjugated secondary antibodies before stimulation, as in Fig. 1A, were measured with Imaris (Bitplane). Endosomes were tracked for 15 min (Early), then 15 min more (Late) after ligand stimulation. (B) Nine representative tracks of data in A (each is a different color), longer than 1 min, for endosomes loaded with fluorescently labeled CCR2B, for each type of cell (shScr and shFLNa), from two independent experiments. (C) Time series of fluorescence micrographs showing FRAP analysis of CCR2B in Rab4A–YFP-loaded endosomes in control (shScr) and shFLNa cells treated as described in A. The 488-nm line was used to follow the Rab4A-positive endosome, and the 633-nm line was used for bleaching an area enclosing the entire endosome (4 μm^2) and for monitoring of receptor fluorescence recovery over 2.5 min. Images were recorded as 16-bit sequences with a pinhole of 246 µm, giving a *z*-slice of 2 µm. Images were acquired at 3-s intervals. Data sets where the endosome moved in the *z*-plane were discarded. Analysis with a control region of interest (ROI) drawn at a certain distance away from the bleached ROI indicated no significant bleaching while fluorescence recovery was monitored. See Fig. S2A for Rab4A–YFP FRAP control. (D) Graphs showing the mobile fraction of CCR2B (left) and Rab4A (right) quantified from 50 endosomes from different cells as described in C. *n*=4 independent experiments. See also Movie 1. Data are means±s.e.m. (**P*<0.05, ***P*<0.01; ****P*<0.001; two-tailed *t*-test). Imaging was performed with a Leica TCS SP5 using a 63×1.3 NA oil immersion lens.

CCR2B with coronin2 on Rab4A-positive endosomal membranes (Fig. 5A,C). Likewise, depletion of FLNa also diminished β2AR-receptor-loading in coronin2-positive domains (Fig. 5C). These results suggest that FLNa might be required for efficient loading of some GPCRs onto the actin-enriched sorting endosome microdomains.

FLNa is required for efficient CCR2B and β2AR recycling

If FLNa contributes to the concentration of certain GPCRs into domains for subsequent loading of transport intermediates from the sorting endosomes to the plasma membrane, its absence should alter receptor endocytic transport and recycling. We analyzed the recycling kinetics of CCR2B and β2AR in FLNa-depleted cells by using fluorescence microscopy to measure the return of the internalized receptor back to plasma membrane. Consistent with our hypothesis, knocking down FLNa produced a significant delay in the kinetics of the retrograde trafficking of the receptors to the plasma membrane (Fig. 6A,B). Meanwhile, transport of the Tfn receptor through the short or long recycling routes was unaffected in shFLNa cells (Fig. 6C,D), as shown previously (Mayor et al., 1993). Internal Tfn was normalized for the time 0 after the first stripping. The data strongly indicated that general membrane traffic from the endosomes to the cell surface was unaffected in FLNa-depleted cells, but rather that FLNa depletion specifically altered the transport of certain cargo.

Our data strongly indicate that FLNa acts as a trafficking adaptor rather than as a structural protein during endosomal trafficking to the plasma membrane. To further investigate this matter, we next asked whether the FLNa regulation of CCR2B recycling involved the FLNa actin-binding domain (ABD), which forms the orthogonal actin networks (Janmey et al., 1990). Strikingly and consistent with our hypothesis, the mouse mutant construct FLNa-ABD–DsRed, with the actin-binding domain deleted (Muriel et al., 2011), resulted in a similar level of receptor recycling to that with wild-type mouse FLNa (Fig. 6E; Fig. S3A). Confocal micrographs of mouse FLNa-ABD–DsRed denoted a prominent cytoplasmic distribution of the mutant, which hindered its visibility on vacuolar structures, which nevertheless could still be observed in some cells (Fig. S3A). These results suggest that the predominant actin cross-linking activity of FLNa might not be an important function of the protein in CCR2B recycling; however, we cannot completely rule out the possibility that the second actin-binding domain of FLNa that has been reported previously (Nakamura et al., 2007) is sufficient for receptor recycling. These results agree with our previous observations that FLNa does not affect actin–coronin2 patches but might facilitate loading of certain receptors into these microdomains.

FLNa is phosphorylated at multiple sites by several protein kinases (Nakamura et al., 2011). Among these, phosphorylation at residue S2152 (Muriel et al., 2011; Tigges et al., 2003; Travis et al., 2004) has a clear impact on FLNa function. To study whether FLNa

Journal of Cell Science (2017) 130, 490-501 doi:10.1242/jcs.193821

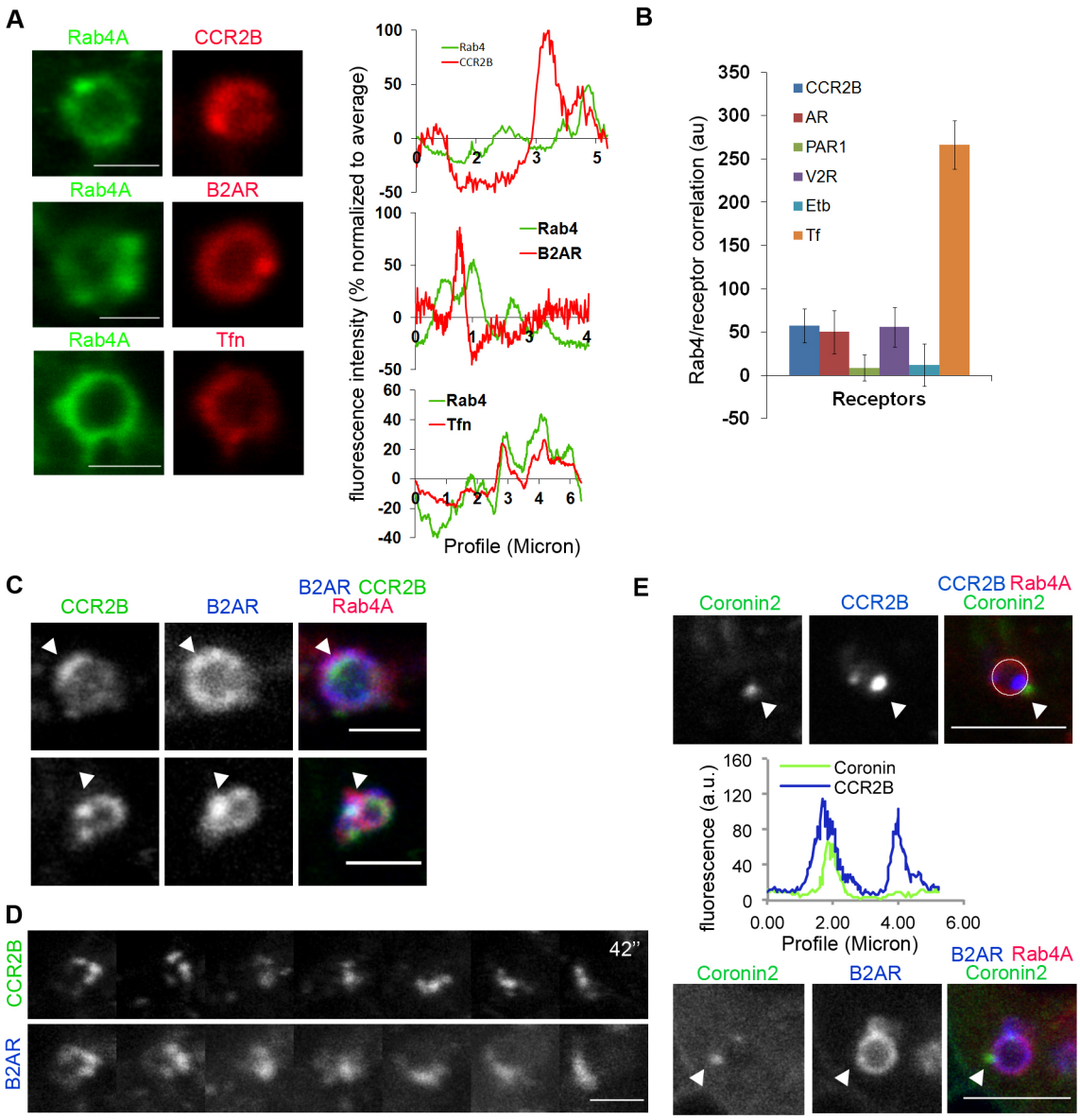

Fig. 3. CCR2B colocalized with β2AR in coronin2-enriched microdomains. (A) HEK293 cells that had been transiently transfected with Rab4A–YFP and Flag–CCR2B, Flag–β2AR, Flag–V2R (see images Fig. S2B), Flag–EtB (see images Fig. S2B) or Flag–PAR1 (see images Fig. S2B) were pre-labeled with anti-Flag and Alexa-Fluor-647-conjugated anti-mouse antibodies, and induced to internalize with addition of the corresponding ligands or Alexa-Fluor-647–Tfn-receptor and were imaged. Zoomed images of individual endosomes are shown. Right, fluorescence intensity profiles of receptors together with that of Rab4A–YFP. (B) Quantification of the Pearson correlation profiles obtained from a minimum of eight endosomes in at least three independent experiments from A. AR, β2AR; Tf, transferrin. (C) Micrographs of endosomal structures of live HEK293 cells expressing Rab4–Cherry, Flag–CCR2B and HA–β2AR that had been surface-labeled with anti-Flag and anti-HA antibodies, followed by anti-mouse Alexa-Fluor-488- and anti-rat Alexa-Fluor-647-conjugated antibodies. Cells were treated with 20 nM CCL2 and 10 µM isoproterenol before acquisition of images as in Fig. 1A. Arrowheads show colocalization of HA–β2AR and CCR2B. (D) Time-lapse series from a representative endosome with Flag–CCR2B and HA–β2AR from C. (E) Confocal images of live cells that expressed coronin2–GFP and Flag–CCR2B (up) or HA–β2AR (down) in Rab4A–Cherry-HeLa transfected cells. The cells were pre-labeled with anti-Flag and anti-mouse Alexa-Fluor-647-conjugated antibodies, or anti-HA and anti-rat Alexa-Fluor-647-conjugated antibodies. Cells were treated with 20 nM CCL2 or 10 µM isoproterenol before acquisition of images as in Fig. 1A. Arrowheads show colocalization of receptors with coronin2. Scale bars: 5 µm. In the middle panel, fluorescence intensity profiles of CCR2B together with coronin2-GFP are shown, as in A.

phosphorylation is required to sustain CCR2B recycling, we analyzed the capacity of FLNa-S2152 mutants to revert receptor recycling defects in FLNa-knockdown cells by using flow cytometry to analyze shFLNa cells (Fig. 6E). Western blot analysis demonstrated that all constructs and mutants (regardless of whether they were tagged with GFP or DsRed) were expressed at similar levels (Fig. 6E,F, upper panels). We observed that the phosphorylation mimetic FLNa mutant, S2152E, supported receptor recycling similar to wild-type FLNa. However, the non-phosphorylatable FLNa-S2152A mutant only partially recovered CCR2B recycling. Consistent with this, the phospho-mimetic mutant (FLNa-S2152E–DsRed or FLNa-S2152E–GFP) was present on endosomal membranes (Fig. 6F; Fig. S3A,B), whereas the GFP- or DsRed-tagged FLNa-S1252A mutant could hardly be detected on these organelles (Fig. 6F; Fig S3A,B). This was despite the fact that both mutants were present at the cellular cortex

Journal of Cell Science (2017) 130, 490-501 doi:10.1242/jcs.193821

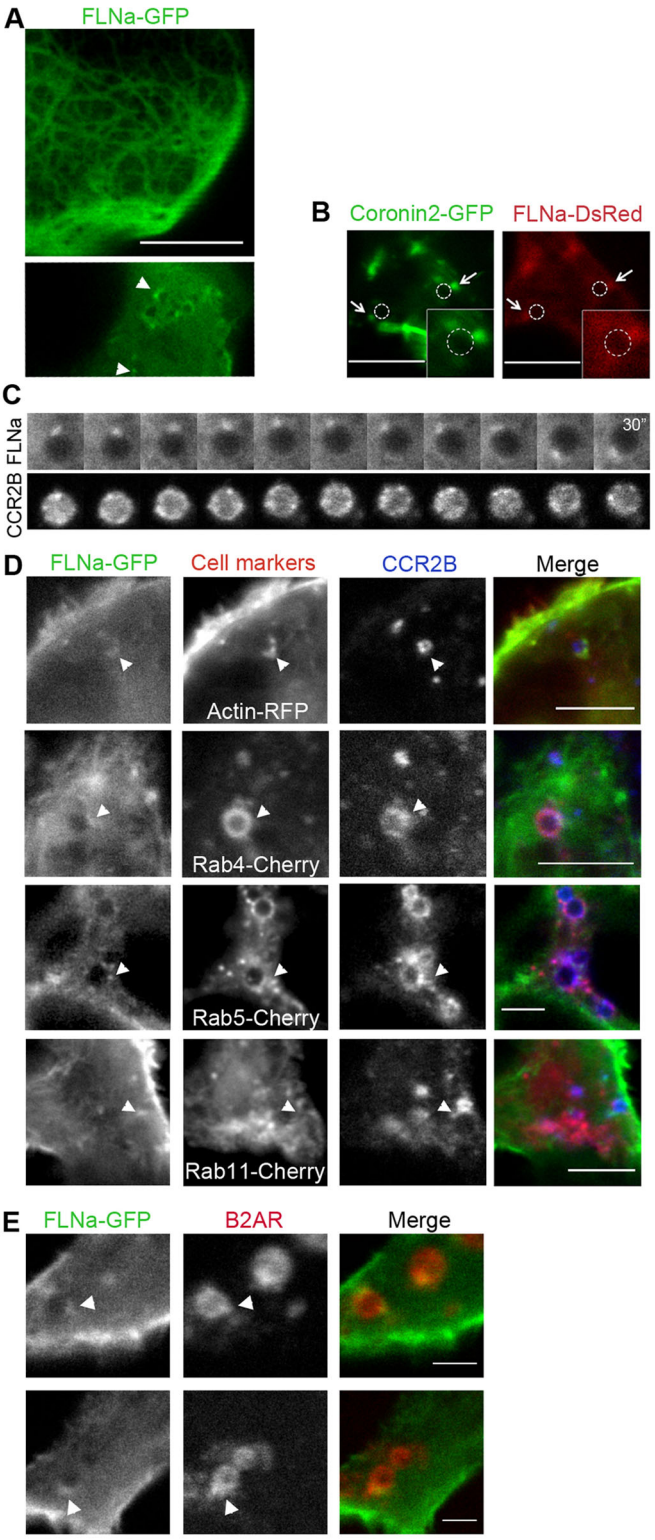

Fig. 4. FLNa and CCR2B colocalized in actin- and coronin2-enriched microdomains. (A) Micrographs from FLNa–GFP-expressing HEK293 cells that had been scanned with a high-resolution STED microscope, showing the filament pattern at the top and vesicular structures in the sagittal plane (bottom). Arrowheads show FLNa in vesicular structures. (B) Live confocal images of coronin2–GFP- and FLNa–DsRed-expressing HeLa cells. Images were taken as described in Fig. 1A. Arrows show colocalization of FLNa and coronin2. (C) Time-lapse series from a representative Rab4A–Cherry-labeled endosome with FLNa–GFP and Flag–CCR2B in transfected HeLa cells that had been prelabeled with anti-Flag and Alexa-Fluor-647-conjugated anti-mouse antibodies, treated as in Fig. 1A. (D) Confocal images of live Flag–CCR2B-expressing HeLa cells that also expressed FLNa–GFP or other cell markers (actin–RFP, Rab4A–Cherry, Rab5A–Cherry or Rab11A–Cherry). Cells were treated and imaged as in C for 30 min at 37°C. Arrowheads indicate FLNa in endosome microdomains. The movies from which images in D were taken are in Movies 2–4. (E) Confocal micrographs of HEK293 cells expressing HA–β2AR (HA–B2AR) and FLNa–GFP that had been surface labeled with anti-HA and anti-rat Alexa-Fluor-568-conjugated antibodies, and treated with 10 µM isoproterenol before acquisition of images. Scale bars: 5 µm.

(Fig S3B,C). This suggests that phosphorylation of FLNa at residue S2152 regulates its localization on endosomal structures.

CCR2 and β2AR signaling induces phosphorylation of FLNa at S2152

We also investigated whether the activation of CCR2B could itself induce FLNa phosphorylation as a mechanism to control its own trafficking. For this, we utilized a specific antibody against FLNa phosphorylated at S2152. The specificity of the antibody was validated by immunoblot analysis of cells expressing the FLNa-S2152A–GFP mutant in shFLNa-transfected HEK293 cells (Fig. 7A). Only the wild-type form of FLNa but not the FLNa-S2152A mutant was detected by the antibody. Notice that only the long form of FLNa–GFP that contained the phosphorylation site was recognized by the antibody (Fig.7A, see arrows). Treatment with CCL2 induced a small but significant increase in FLNa phosphorylation, 5 and 15 min after CCL2 stimulation (Fig. 7B), which paralleled the activation of ERK by CCL2 (Fig. S4A–C). CCL2 did not induce any increase in phosphorylation of the FLNa-S2152A mutant that had been expressed in shFLNa HEK293 cells (Fig. 7A, lower panel). Different kinases have been implicated in the phosphorylation of FLNa, including several isoforms of PKC and PKA, which are also downstream effectors of GPCR signaling. Treatment with different protein kinase inhibitors targeting PKCs [GF10903, Gö6976 and bisindolylmaleimide II] (Fig. 7C–E) consistently produced a significant reduction of FLNa phosphorylation at S2152 upon CCL2 treatment. The reduction of phosphorylation of FLNa at S2152 in CCL2-stimulated cells upon treatment with GF10903 was dose dependent (Fig. 7D). In contrast, no inhibition of FLNa phosphorylation at S2152 was observed in the presence of the PKA inhibitor H-89, even at relatively high doses. β2AR stimulation also led to FLNa phosphorylation on S2152 after 5 and 15 min of isoproterenol treatment (Fig. 7F,G). Interestingly, however, phosphorylation of FLNa at S2152 induced by β2AR was not reduced in the presence of GF10903 but on the contrary, it was reduced in the presence of H-89. Again, isoproterenol stimulation did not result in any phosphorylation of the FLNa-S2152A mutant (Fig. 7F). Therefore, we can conclude that both receptors, CCR2B and β2AR, can induce phosphorylation of FLNa at S2152 upon ligand stimulation, most probably through different downstream pathways.

DISCUSSION

Our work demonstrates a very specific role of FLNa in promoting the recycling of CCR2B from sorting endosomes to the plasma membrane. We showed that FLNa and internalized CCR2B colocalized in dynamic actin- and coronin2-enriched endosomal subdomains, which are known to concentrate cargo for the Rab4A- and retromer-dependent pathway to the plasma membrane (Puthenveedu et al., 2010; Temkin et al., 2011), which is also used by other GPCRs like β2AR and AVPR2 (V2R). Interestingly, even though filamins have a prominent role as actin cross-linkers, we also

Journal of Cell Science (2017) 130, 490-501 doi:10.1242/jcs.193821

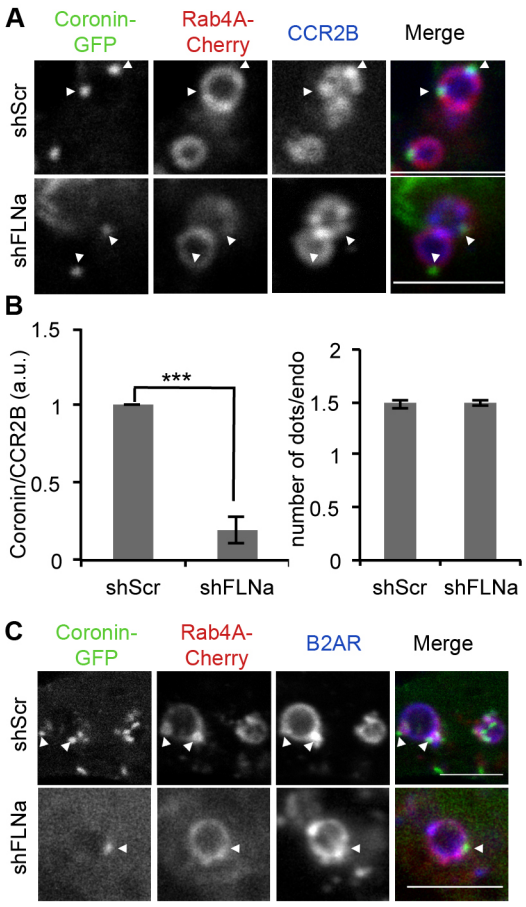

Fig. 5. FLNa facilitates CCR2B loading in actin-rich subdomains. (A) Micrographs of endosomes in shFLNa or shScr cells that expressed Flag–CCR2B, Rab4A–Cherry and coronin2–GFP. Cells were treated as described in Fig. 3E. Arrowheads show coronin2–GFP localization. (B) Correlation of coronin2 with CCR2B on the endosomes shown in A (left panel). The tool 'Plot profile' of a free-hand-drawn line on the endosomal membrane was used to calculate correlations between the two signals according to the Pearson's correlation. Right, mean number of coronin2–GFP patches on CCR2-loaded endosomes±s.e.m. of three independent experiments (***P<0.001; two-tailed t-test). 20 endosomes were counted per experiment. endo, endosome. (C) Micrographs of endosomes in shFLNa or shScr cells that expressed Flag–β2AR, Rab4A–Cherry and coronin2–GFP. Cells were treated as described in Fig. 3C. Arrowheads show coronin2–GFP localization. Scale bars: 5 µm.

found that FLNa does not seem to play a major structural role in organizing the endosomal actin-enriched microdomains, but rather that it functions as a cargo adaptor. We showed that FLNa depletion does not apparently alter the size or number of the endosomal coronin2 microdomains, nor did it affect overall retrograde traffic, but rather it specifically prevented CCR2B and β2AR loading onto the actin-enriched microdomains and specifically delayed their transport back to the plasma membrane. Also consistent with this view, the actin-binding site of FLNa that is responsible for its actin cross-linking activity was not required to sustain efficient recycling of CCR2B and β2AR. Based on our current observations and previous data demonstrating that FLNa interacts with several chemokine receptors and integrins (Liu et al., 2015), which follow the same path to the plasma membrane, we propose that FLNa works as a receptor scaffold that links cargo directly or indirectly to actin microdomains in the sorting endosome. We found that this FLNa function is regulated by its phosphorylation at S2152, which, in turn, is promoted by GPCR-signaling to second messenger kinases.

In addition to a direct role of FLNa in CCR2B and β2AR recycling, our data demonstrated that FLNa depletion greatly reduced the long-term motility of the sorting endosomes and increased their size. Depletion of WASH (Gomez et al., 2012), or the Arp2/3 complex (Derivery et al., 2012), also causes early endosome enlargement. In these conditions, endosomes present enlarged segregated subdomains with collapsed endosomal and lysosomal networks. They do not exhibit elongated tubulations and are devoid of filamentous actin. Although FLNa depletion increased the endosome size, it did not seem to alter the actin-rich endosome domains, as the number and size of the coronin2 patches remained the same and no collapse of endosomal networks was observed, which suggest that role of FLNa differs from that seen in WASH and Arp2/3 studies. Whether the endosomal phenotypes observed by FLNa depletion are a cause or a consequence of the recycling defect, or are unrelated, is a complex question to address in the future. Thus, a defect in the recycling of certain cargo might prevent maturation of endosomes and their proper attachment to microtubules for long-range movement. Reciprocally, the enlargement of endosomes might be caused not only by the accumulation of certain cargo unable to exit the organelle but also by maintenance of the endosome capacity to accept vesicles from the plasma membrane, provided that they do not move away from the cortex. Alternatively, or additionally, depletion of FLNa might directly alter tubulin-based motility, or the architecture of microtubules (Lynch et al., 2011), and as a consequence, indirectly affect endosomal motility, size and distribution (Bayer et al., 1998) without having a dramatic effect on the actin cytoskeleton structure (Baldassarre et al., 2009). In any case, a general alteration of the endosome motility or distribution is unlikely to be the primary cause of the CCR2B recycling defects because the kinetics of Tfn transport from the endosomes to plasma membrane appeared to be unaltered in FLNa-depleted cells (Fig. 6C,D; Minsaas et al., 2010), as did its uptake (Muriel et al., 2011). We favor the hypothesis that FLNa acts as a scaffold that cooperates to load the cargo into actin-enriched domains. Concomitantly, FLNa would be needed to maintain the distribution and motility of endosomes by interacting with actin and/or microtubule networks. This hypothesis agrees with our previous results showing that upon activation, CCR2B-loaded vesicles were present in a linear distribution with directional movement, co-aligned with actin fibers and FLNa (Minsaas et al., 2010; Planagumà et al., 2012). It is interesting that FLNa regulates the linear distribution of caveolae along stress fibers (Muriel et al., 2011) and their translocation from the plasma membrane to perinuclear Rab11 structures.

FLNa is regulated by phosphorylation at S2152 by many protein kinases, and this phosphorylation has a direct effect on its function in regulating a variety of cytoskeleton-related events (Hastie et al., 1997; Muriel et al., 2011; Travis et al., 2004; Zhang et al., 2012). Here, we show that phosphorylation of the same residue is necessary for efficient recycling of CCR2B and β2AR. Together with the fact that the S2152A mutant of FLNa was not present in endosomes, our data suggest that phosphorylation of FLNa at S2152 facilitates the accumulation of this protein on endosomal microdomains (see model in Fig. 7I). These results agree with previous data where Myc-tagged FLNa-S2152A localizes with actin fibers at the cell surface, whereas phosphorylation of FLNa directs it towards the cytoplasm of CHP100 cells (Zhang et al., 2012). We also showed here that CCR2B and β2AR signaling can trigger phosphorylation of FLNa at S2152. Interestingly, our data also suggests that phosphorylation of FLNa at S2152 by these GPCRs follows different pathways and uses different kinases because CCR2-

Journal of Cell Science (2017) 130, 490-501 doi:10.1242/jcs.193821

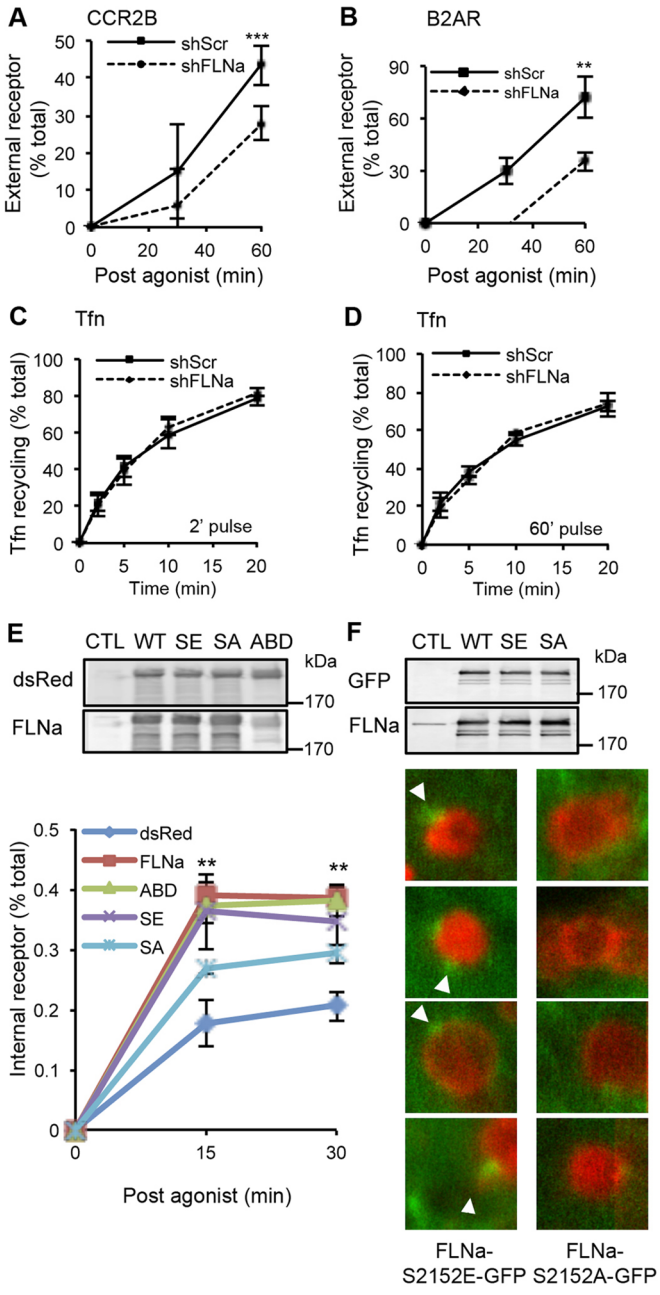

Fig. 6. Recycling of GPCRs is markedly delayed in FLNa-deficient HeLa cells. Graph showing the percentage of internalized CCR2B (A) and β2AR (B) that was recycled back to the plasma membrane. HeLa cells expressing Flag–CCR2B or β2AR that had been surface labeled with anti-Flag antibody and stimulated with 20 nM CCL2 or 10 µM isoproterenol for 15 min at 37°C were acid-washed and tracked for the times indicated. Cells were then fixed and incubated with Alexa-Fluor-647-conjugated antibody exclusively, just detecting recycled receptors at the plasma membrane. Fluorescence was quantified for *n*=4 independent experiments with a minimum of eight cells for each experiment and normalized to values at time 0. Acquired image sequences were saved as 16-bit stacks and quantified using FiJi. Data are means±s.e.m., shScr versus shFLNa at 60 min in A and B (***P*<0.01, ****P*<0.001, two-tailed *t*-test). (C,D) Flow cytometry analysis of HEK293 cells for the recycling of Alexa-Fluor-568-conjugated Tfn (0.02 mg/ml) after 2 and 60 min pulses. Cells were then chased for the indicated times. The percentage of transferrin recycled was calculated as 1 minus the internal fluorescence values multiplied by 100. Data are averaged from at least three independent experiments and shown the mean ±s.e.m. (E) Flow cytometry analysis of Flag–CCR2B recycling in shFLNa cells that had been complemented with the following mouse shFLNa-insensitive constructs: FLNa–DsRed, FLNa-S2152E–DsRed (SE), FLNa-S2152A–DsRed (SA) or FLNa-ABD–DsRed (ABD). Cells that had been surface labeled with anti-Flag antibody conjugated to Alexa-Fluor-488 were induced to internalize receptors with 20 nM CCL2 for 15 min, acid-washed and processed for flow cytometry analysis. Internal receptor was normalized to that at time 0 after the first stripping. The percentage of antibody recycled was calculated as 1 minus the internal fluorescence values. The upper panel shows immunoblotting of shFLNa cells that expressed DsRed, FLNa–DsRed, FLNa-S2152E–DsRed, FLNa-S2152A–DsRed and FLNa-ABD–DsRed. (F) The upper panel shows immunoblots of shFLNa cells that expressed FLNa–GFP, FLNa-S2152E–GFP and FLNa-S2152A–GFP. The lower images show fluorescence micrographs of CCR2-loaded endosomes of shFLNa cells expressing FLNa-S2152E–GFP or FLNa-S2152A–GFP (treated as described in Fig. 3D). Arrowheads indicate FLNa-positive microdomains in endosomes. Data are means±s.e.m., shScr cells versus FLNa-expressing cells (dark blue line versus red line) (***P*<0.01; two-tailed *t*-test). See Fig. S3 for controls of FLNa mutant expression by immunofluorescence.

induced phosphorylation of FLNa at S2152 was reduced by PKC inhibitors but not by PKA inhibitors. Reciprocally, β2AR-induced phosphorylation relied more on a PKA-dependent pathway. The data are consistent with the different signaling cascades ignited by the different GPCRs, CCR2 relying mainly on G_i and G_q which lead to PKC activation (Janjanam et al., 2015; Jiménez-Sainz et al., 2003), and β2AR on G_s, leading to PKA activation. By contrast, it is well established that FLNa can be phosphorylated at S2152 by cAMP-dependent PKA (Ithychanda et al., 2015; Jay et al., 2004). Moreover, other ligand-activated GPCRs, like angiotensin II type-1 receptor (AT1R), MAS and the α_{1d}-adrenergic receptor, have been shown to enhance PKA-mediated filamin phosphorylation of Ig domains 16–24 *in vitro* (Tirupula et al., 2015). Whether GPCR-induced FLNa phosphorylation at S2152 is directly mediated by PKC cannot be confirmed at this point, but it is possible given that different isoforms of PKC have previously been demonstrated to phosphorylate filamin A *in vitro* (Tigges et al., 2003). Nevertheless, FLNa S2152 is probably phosphorylated by other kinases since inhibitors of PKC or PKA did not completely obliterate CCR2- or β2AR-induced phosphorylation of FLNa at S2152, and this residue has been shown to be phosphorylated by other kinases (Gómez-Moutón et al., 2015). Interestingly, the residue S2152 of FLNa is located in Ig repeat 21, which is usually hidden in the autoinhibited conformation of FLNa (Lad et al., 2007). Filamin A needs to undergo a conformational adjustment for the phosphorylation on S2152 to occur (Ithychanda et al., 2015). Together with our present data, it reinforces the concept that ligand-dependent phosphorylation of FLNa by GPCRs becomes an important pathway for FLNa activation by promoting the phosphorylation of S2152. Overall, we favor the hypothesis that a signaling response leading to activation of different second messenger protein kinases to phosphorylate FLNa, which in turn will induce its detachment from the actin structures at the cell cortex and facilitate its localization in highly dynamic actin-enriched endosomal microdomains (Fig. 7I). This mechanism probably operates for other chemokine receptors and other GPCRs.

MATERIALS AND METHODS

Constructs and reagents

Plasmids encoding FLNa–EGFP, Flag–CCR2B (Planagumà et al., 2012), FLNa-S2152A–DsRed and FLNa-S2152E–DsRed (Muriel et al., 2011) have been described previously. FLNa–DsRed was a gift from David A. Calderwood (Yale School of Medicine, New Haven, CT); FLNa-S2152A–GFP and FLNa-S2152E–GFP were derived from pcDNA3.1-FLNa-EGFP. Human Rab4A–YFP and human Rab5A–GFP were provided by Peter van der Sluijs (University

Journal of Cell Science (2017) 130, 490-501 doi:10.1242/jcs.193821

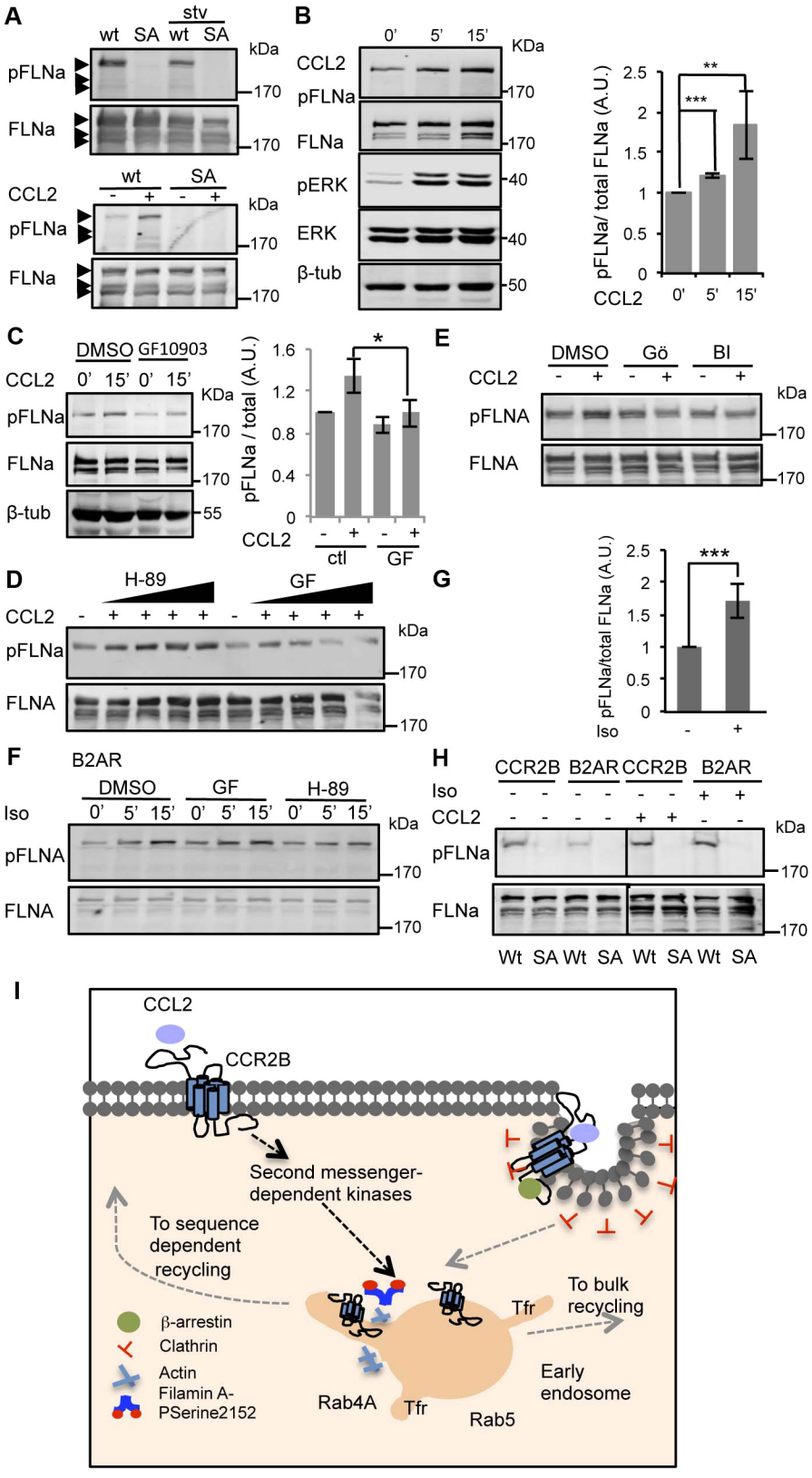

Fig. 7. Phosphorylation of FLNa at S2152 by CCR2 signaling. (A) Validation of the antibody against phosphorylated FLNa (pFLNa). Upper panels, immunoblots for FLNa phosphorylated at S2152 (pFLNa), which were then stripped and reprobed for total FLNa in protein extracts of shFLNa HEK293 cells that expressed FLNa (wt) or FLNa-S2152A (SA) under control or starving conditions (stv). Lower panels, immunoblots against FLNa phosphorylated at S2152, which were then stripped and reprobed for total FLNa in protein extracts of shFLNa HeLa cells expressing Flag–CCR2B together with FLNa or FLNa-S2152A and stimulated with 20 nM CCL2 for 15 min. (B) Immunoblots of HeLa cells that expressed CCR2B were stimulated with 20 nM CCL2 for 5 and 15 min. Lysates were subjected to immunoblotting with antibodies against pFLNa and phosphorylated ERK (pERK), and reprobed with anti-FLNa and anti-ERK 1 and -ERK2 antibodies (ERK) (see Fig. S4 for CCL2-induced pERK assays). β-tub, β-tubulin. (C) HeLa cells were pretreated with 1 µM GF10903 (GF) or DMSO for 1 h and stimulated with 20 nM CCL2 for 5 and 15 min. Graphs (B,C) show the amount of pFLNa (quantified in the linear range with an Odyssey imager) normalized to the corresponding FLNa signal from three different experiments, expressed as the average fold-increase±s.e.m. of FLNA phosphorylation relative to that at time 0 (right panels) (*P<0.05, **P<0.01, ***P<0.001; two-tailed t-test). (D) HeLa cells that had been transfected with CCR2B and pretreated with increasing concentrations of H-89 (0.1, 0.5, 5 and 20 µM) and GF10903 (GF, 0.02, 0.1, 0.5, 1 µM) were stimulated with 20 nM CCL2 for 15 min. (E) Cells as described in D were pretreated with Gö6976 (2 µM) or with bisindolylmaleimide II (BI, 2 µM) or DMSO for 1 h. (F) HeLa cells that had been transfected with Flag–β2AR (B2AR) and pretreated with 1 µM GF10903 and 20 µM H-89 were stimulated with 10 µM isoproterenol (Iso) for the times indicated. (G) A graph showing the quantification of pFLNa after stimulation for 15 min with 10 µM isoproterenol or in cells that had been left unstimulated. (H) shFLNa HEK293 cells that expressed FLNa (wt) or FLNa-S2152A (SA) and had been transfected with Flag–CCR2B and Flag–β2AR (B2AR) were stimulated with 20 nM CCL2 and 10 µM isoproterenol, respectively. (I) A model of homeostatic regulation of CCR2B recycling. Phosphorylation of S2152 of FLNa in response to CCL2 facilitates the entry of CCR2B into actin-positive tubules and its recycling. Tfr, transferrin receptor; pSerine2152, FLNa phosphorylated at S2152.

Medical Center Utrecht, The Netherlands). pCherry-C-hRab4A and pCherry-C-hRab5A were derived from human (h)Rab4A–YFP and hRab5A–GFP (previously sequenced). Actin–RFP was from Stein O. Døskeland (Department of Biomedicine, University of Bergen, Norway). Coronin2–GFP was kindly provided by Manojkumar A. Puthenveedu (Carnegie Mellon University, Pittsburgh, PA). Primary antibodies used were: M1 anti-Flag (#F3040, Sigma; 1/1000 dilution), anti-filamin 1 (E-3; mouse sc-17749, Santa Cruz Biotechnologies; 1/1000 dilution), anti-filamin phosphorylated at S2152 (#4761, Cell Signaling; 1/1000 dilution),

Journal of Cell Science (2017) 130, 490-501 doi:10.1242/jcs.193821

anti-phospho ERK1/2 and anti-ERK1/2 (p44/42 MAPK 137F5 #4695; Cell Signaling; dilution 1/1000), and anti-β-tubulin (#T6199, Sigma; 1/1000 dilution) antibodies. Alexa-Fluor-647- (#A21245, lot#651740; #A21236, lot# 716822) and Alexa-Fluor-488-conjugated (anti-mouse #A21202, lot #536050) secondary antibodies were from Invitrogen (all used at 1:1000 dilution). CF488A- and CF568-labeled M1 anti-Flag antibodies (Sigma-Aldrich) were obtained with Mix-n-Stain™ CF™ Antibody Labeling Kit (MX488AS100-1KT, Sigma-Aldrich) following the manufacturer's instructions. A mouse anti-EEA-1 antibody (#610457, BD Transduction Laboratories) was detected by an anti-rabbit secondary antibody after treating first the antibody with Affinity Pure Fab Fragment Rabbit Anti-Mouse IgG (H+L) according to the manufacturer's instructions (#315-007-003, Jackson ImmunoResearch). For western blot infrared analysis (Odyssey, LI-COR), IRDye680- and IRDye800-conjugated anti-rabbit and anti-mouse secondary antibodies were used (800CW anti-rabbit #926-32311; 800CW anti-mouse #926-32210, lot #C1102603 from Odyssey; anti-rabbit IRDye 680RD #926-68073, lot# C30724-04 from Odyssey, all used at 1:20000 dilution). CCL2 and human MCP-1 were from PeproTech (Rocky Hill, NJ); [Arg^8]-vasopressin acetate salt and endothelin 1 were purchased from Sigma-Aldrich and isoproterenol was obtained from Calbiochem.

Cell treatments and western blotting

HeLa cells were obtained from American Type Culture Collection and always kept under low passage number from the initial clone. HEK293 (293-EBNA) were bought from Life Technologies and cultured in the presence of G418. All cells were grown in Dulbecco's modified Eagle's medium (DMEM) supplemented with 10% (v/v) fetal bovine serum in a humidified atmosphere under 5% CO_2. Cells were regularly tested for mycoplasma contamination. All cells were grown and transfected utilizing FuGene® 6 (Roche) in all experiments. Cells were treated with 20 nM of CCL2 or 10 µM isoproterenol in culture medium for 5 and 15 min prior to analysis. The following concentrations of ligands were also used: 1 µM vasopressin and 10 nM endothelin. For protein kinase inhibition, cells were treated with varying concentrations of GF109203X (inhibitor of PKCα, βI, βII and γ subtypes) (ENZO Life Sciences), H-89 (general inhibitor of protein kinase A), 2 µM Gö6976 (PKCα and PKCβ inhibitor) (Sigma-Aldrich) or 2 µM bisindolylmaleimide II (general PKC inhibitor) (Calbiochem) for 60 min. Utilizing the MISSION shRNA human system (Sigma-Aldrich), FLNa shRNA (shRNA) against human FLNa (TRCN0000062528 and TRCN0000062529) was used in HeLa and HEK293 cells. Virus production was performed as described previously (Masià-Balagué et al., 2015). Cells were solubilized in *N*-dodecyl-D-maltoside buffer (20 mM Tris-HCl, pH 7.5, 150 mM NaCl, 10 mM $MgCl_2$, 1% *N*-D-maltoside, 10 mM NaF, 1 mM Na_3VO_4 and protease inhibitors), as described previously (Masià-Balagué et al., 2015). The same amount of protein was loaded for each condition (measured by BioRad protein assay). Western blots were visualized and quantified by performing infrared detection (Odyssey System) in the linear range.

Cell imaging

For live imaging, HeLa or HEK293 cells that had been transiently transfected with FLNa–GFP, FLNa–GFP-S2152A, -S2152E, Rab4A–Cherry, Rab5–Cherry, Rab11–Cherry, actin–RFP and/or coronin2–GFP and Flag-tagged CCR2B receptors were plated on glass chambers and imaged after addition of anti-Flag antibody for 15 min at 4°C followed by an incubation with anti-mouse Alexa-Fluor-647-conjugated antibody (surface labeled) for 15 min at 4°C before addition of ligand at 37°C. HEK293 cells were also transfected with plasmids encoding Flag-tagged receptors: β2AR, Etb, V2R or PAR1. HA–β2AR was transiently transfected into HEK293 cells with Flag–CCR2B. Confocal imaging was performed with a Leica TCS SP5 (Leica Microsystems, Mannheim, Germany) by using a 63×1.3 NA oil immersion lens in a sealed chamber with 5% CO_2 at 37°C. Movies were taken between 5 and 30 min after agonist addition. Each frame corresponds to 600 ms. For high-resolution fluorescence imaging, a STED microscope (Leica Microsystems) was utilized on live HeLa cells that expressed FLNa–GFP. For fixed cell imaging, HEK293 cells that had been transiently transfected with Flag–CCR2B and plated on glass chambers were treated with CCL2 (20 nM) for 15 or 30 min at 37°C before fixation, and processed for immunofluorescent staining (Planagumà et al., 2012). After fixation and permeabilization, cells were incubated with anti-Flag and anti-EEA-1 antibodies, followed by incubation with the corresponding Alexa-Fluor-conjugated secondary antibodies (as stated in each figure legend).

Fluorescence recovery after photobleaching

Live-cell confocal imaging was performed on transiently transfected Rab4A–Cherry and/or Flag–CCR2B (surface labeled) control (scrambled shRNA) and shFLNa HEK293 cells at 37°C. Images were recorded as 16-bit sequences with a pinhole of 246 µm, giving a *z*-slice of 2 µm, and acquired at 3-s intervals. A 100-mW LASOS argon laser, set to 25% intensity, was used to photobleach a Rab4A endosome, and recovery was monitored for 26 cycles (10 s) with reduced laser power. A 488-nm line was used to follow the Rab4A-positive endosome and a 633-nm line was used to bleach the entire CCR2B endosome (4 µm^2). Monitoring of receptor fluorescence recovery was done for 2.5 min. The mobile fraction (MF) was estimated as $MF=(F_i–F_b)/(F_0–F_b)*100$, where F_i is the final intensity upon recovery over the period of the experiment, F_0 is the intensity before bleaching, and F_b is the intensity immediately after bleaching. Data were analyzed for 50 endosomes under each condition and were acquired on three different days. The background was subtracted and corrected by measuring the fluorescence decay of a non-bleached area in the same cell and normalized to the Rab4A signal (Rabut and Ellenberg, 2005).

Recycling assays

Quantification of receptor recycling was performed as previously described (Patel et al., 2011) using confocal microscopy. Cells that expressed Flag–CCR2B or Flag–β2AR were incubated with anti-Flag antibody at 4°C for 15 min, and endocytosis was initiated by addition of CCL2 or isoproterenol for 15 min at 37°C. Cells were acid-washed to eliminate traces of the antibody bound to the cell surface receptor and allowed to recover with DMEM for various time periods, washed with ice-cold PBS-Ca^{2+}, fixed and incubated with Alexa-Fluor-647-conjugated antibody without permeabilization. Fluorescence intensities were averaged over individual cells and analyzed using the FiJi distribution of ImageJ. In each experiment, a minimum of four replicates were analyzed for each condition. The percentage of antibody that was recycled to plasma membrane was calculated as 1 minus the internal fluorescence values and was normalized against values at time 0 (post agonist) (results in Fig. 6A,B).

For the Tfn flow-cytometry-based recycling assay, HeLa cells were incubated with Alexa-Fluor-568-labeled Tfn at 0.02 mg/ml for 2 or 60 min at 37°C to allow internalization. At 2 min, only early endosomes are loaded with Tfn, and the kinetics of short-loop recycling can be measured. At 60 min, mainly recycling endosomes are loaded with Tfn and, therefore, traffic from the recycling endosomes is mostly measured. After acid stripping, to eliminate surface-bound fluorescent Tfn, the internalized fraction was chased at 37°C with 2 mg/ml of unlabeled Tfn for the indicated times. At each time point, cells were acid-washed, washed with ice-cold PBS and immediately detached using trypsin. Fluorescence intensity profiles of cell populations (10,000 cells per sample) were measured using a FacsAria I SORP (Becton Dickinson, San Jose, CA). Internal Tfn was normalized for the time 0 after the first stripping. The percentage of Tfn recycled was calculated as 1 minus the internal fluorescence values.

Analysis of CCR2B recycling was performed in HEK293 shFLNa cells that had been transiently expressing mouse FLNa–DsRed to rescue the recycling delay, and also cells expressing FLNa-ABD–DsRed, FLNa-S152A–DsRed and FLNa-S2152E–DsRed (Fig. 6E). Conjugation of

anti-Flag M1 antibodies with CF488 was performed following the manufacturer's instructions (Sigma-Aldrich). Conjugated CF488A–M1 anti-Flag antibody was incubated with cells for 15 min at 4°C prior to addition of 20 nM CCL2 and incubation for 15 min at 37°C to allow internalization. Then, cells were acid-washed and allowed to recycle back the receptor to the plasma membrane for the indicated times. Cells were again acid-washed, to exclusively eliminate the antibodies attached to the receptors reaching the plasma membrane, and trypsinized before analysis using a FacsAria I SORP instrument (Becton Dickinson). Green fluorescence intensity profiles were measured only in cell populations that expressed DsRed (5000 cells per sample). The fluorescence intensity measured is then a reflection of internalized receptor that remained intracellularly, which decreased with time upon chase.

Statistical analysis

Data are presented as mean values or as fold induction±s.e.m. as indicated in each figure legend. The sum of all the individual stimulatory effects were compared to that of the combined effects by using the unpaired *t*-test with two-tailed *P*-values, or one-way ANOVA (Fig. 1B) or two-way ANOVA (Fig. 1D) with GraphPad Prism. Differences were considered statistically significant when $*P<0.05$, $**P<0.01$ and $***P<0.001$.

Acknowledgements

We thank E. Rebollo, T. Zimmerman (Centre for Genomic Regulation, Barcelona, Spain), A. Echarri [Centro Nacional de Investigaciones Cardiovasculares, Barcelona, Spain (CNIC)] and D. M. Pavón (CNIC) for scientific and technical assistance, and D. A. Calderwood for providing FLNa–DsRed.

Competing interests

The authors declare no competing or financial interests.

Author contributions

M.P., M.I.G., I.I. and A.M.A. conceived the research and designed the experiments; M.P., G.G., I.I., M.A.-C., J.P., O.M. performed experiments and analyzed data; M.P. and J.P. performed immunofluorescence experiments; M.d.P. provided reagents and designed experiments; M.P., M.I.G. and A.M.A. wrote the manuscript; and all authors read, added comments, and approved manuscript.

Funding

This work was supported by grants from Ministerio de Economía y Competitividad (BFU2011-30080 and BFU2014-53978-R); and Agència de Gestió d'Ajuts Universitaris i de Recerca (SGR41635). G.G. and I.I. were supported by Investigator Research Fellowships (Agéncia de Gestió d'Ajuts Universitaris i de Recerca).

Supplementary information

Supplementary information available online at
http://jcs.biologists.org/lookup/doi/10.1242/jcs.193821.supplemental

References

Awata, H., Huang, C., Handlogten, M. E. and Miller, R. T. (2001). Interaction of the calcium-sensing receptor and filamin, a potential scaffolding protein. *J. Biol. Chem.* **276**, 34871-34879.

Baldassarre, M., Razinia, Z., Burande, C. F., Lamsoul, I., Lutz, P. G. and Calderwood, D. A. (2009). Filamins regulate cell spreading and initiation of cell migration. *PLoS ONE* **4**, e7830.

Bayer, N., Schober, D., Prchla, E., Murphy, R. F., Blaas, D. and Fuchs, R. (1998). Effect of bafilomycin A1 and nocodazole on endocytic transport in HeLa cells: implications for viral uncoating and infection. *J. Virol.* **72**, 9645-9655.

Bose, S. and Cho, J. (2013). Role of chemokine CCL2 and its receptor CCR2 in neurodegenerative diseases. *Arch. Pharm. Res.* **36**, 1039-1050.

Cao, T. T., Deacon, H. W., Reczek, D., Bretscher, A. and von Zastrow, M. (1999). A kinase-regulated PDZ-domain interaction controls endocytic sorting of the beta2-adrenergic receptor. *Nature* **401**, 286-290.

Cho, E.-Y., Cho, D.-I., Park, J. H., Kurose, H., Caron, M. G. and Kim, K.-M. (2007). Roles of protein kinase C and actin-binding protein 280 in the regulation of intracellular trafficking of dopamine D3 receptor. *Mol. Endocrinol.* **21**, 2242-2254.

Derivery, E., Sousa, C., Gautier, J. J., Lombard, B., Loew, D. and Gautreau, A. (2009). The Arp2/3 activator WASH controls the fission of endosomes through a large multiprotein complex. *Dev. Cell* **17**, 712-723.

Derivery, E., Helfer, E., Henriot, V. and Gautreau, A. (2012). Actin polymerization controls the organization of WASH domains at the surface of endosomes. *PLoS ONE* **7**, e39774.

Deshmane, S. L., Kremlev, S., Amini, S. and Sawaya, B. E. (2009). Monocyte chemoattractant protein-1 (MCP-1): an overview. *J. Interferon Cytokine Res.* **29**, 313-326.

García Lopez, M. A., Aguado Martínez, A., Lamaze, C., Martínez-A, C. and Fischer, T. (2009). Inhibition of dynamin prevents CCL2-mediated endocytosis of CCR2 and activation of ERK1/2. *Cell. Signal.* **21**, 1748-1757.

Gomez, T. S. and Billadeau, D. D. (2009). A FAM21-containing WASH complex regulates retromer-dependent sorting. *Dev. Cell* **17**, 699-711.

Gomez, T. S., Gorman, J. A., de Narvajas, A. A.-M., Koenig, A. O. and Billadeau, D. D. (2012). Trafficking defects in WASH-knockout fibroblasts originate from collapsed endosomal and lysosomal networks. *Mol. Biol. Cell* **23**, 3215-3228.

Gómez-Moutón, C., Fischer, T., Peregil, R. M., Jiménez-Baranda, S., Stossel, T. P., Nakamura, F. and Mañes, S. (2015). Filamin A interaction with the CXCR4 third intracellular loop regulates endocytosis and signaling of WT and WHIM-like receptors. *Blood* **125**, 1116-1125.

Hartwig, J. H., Tyler, J. and Stossel, T. P. (1980). Actin-binding protein promotes the bipolar and perpendicular branching of actin filaments. *J. Cell Biol.* **87**, 841-848.

Hastie, L. E., Patton, W. F., Hechtman, H. B. and Shepro, D. (1997). H2O2-induced filamin redistribution in endothelial cells is modulated by the cyclic AMP-dependent protein kinase pathway. *J. Cell. Physiol.* **172**, 373-381.

Ithychanda, S. S., Fang, X., Mohan, M. L., Zhu, L., Tirupula, K. C., Naga Prasad, S. V., Wang, Y.-X., Karnik, S. S. and Qin, J. (2015). A mechanism of global shape-dependent recognition and phosphorylation of filamin by protein kinase A. *J. Biol. Chem.* **290**, 8527-8538.

Janjanam, J., Chandaka, G. K., Kotla, S. and Rao, G. N. (2015). PLCβ3 mediates cortactin interaction with WAVE2 in MCP1-induced actin polymerization and cell migration. *Mol. Biol. Cell* **26**, 4589-4606.

Janmey, P. A., Hvidt, S., Lamb, J. and Stossel, T. P. (1990). Resemblance of actin-binding protein/actin gels to covalently crosslinked networks. *Nature* **345**, 89-92.

Jay, D., García, E. J. and de la Luz Ibarra, M. (2004). In situ determination of a PKA phosphorylation site in the C-terminal region of filamin. *Mol. Cell. Biochem.* **260**, 49-53.

Jiménez-Baranda, S., Gómez-Moutón, C., Rojas, A., Martínez-Prats, L., Mira, E., Ana Lacalle, R., Valencia, A., Dimitrov, D. S., Viola, A., Delgado, R. et al. (2007). Filamin-A regulates actin-dependent clustering of HIV receptors. *Nat. Cell Biol.* **9**, 838-846.

Jiménez-Sainz, M. C., Fast, B., Mayor, F. and Aragay, A. M. (2003). Signaling pathways for monocyte chemoattractant protein 1-mediated extracellular signal-regulated kinase activation. *Mol. Pharmacol.* **64**, 773-782.

Johnson, Z., Schwarz, M., Power, C. A., Wells, T. N. C. and Proudfoot, A. E. I. (2005). Multi-faceted strategies to combat disease by interference with the chemokine system. *Trends Immunol.* **26**, 268-274.

Kim, K.-M., Gainetdinov, R. R., Laporte, S. A., Caron, M. G. and Barak, L. S. (2005). G protein-coupled receptor kinase regulates dopamine D3 receptor signaling by modulating the stability of a receptor-filamin-beta-arrestin complex. A case of autoreceptor regulation. *J. Biol. Chem.* **280**, 12774-12780.

Lad, Y., Kiema, T., Jiang, P., Pentikäinen, O. T., Coles, C. H., Campbell, I. D., Calderwood, D. A. and Ylänne, J. (2007). Structure of three tandem filamin domains reveals auto-inhibition of ligand binding. *EMBO J.* **26**, 3993-4004.

Liu, J., Das, M., Yang, J., Ithychanda, S. S., Yakubenko, V. P., Plow, E. F. and Qin, J. (2015). Structural mechanism of integrin inactivation by filamin. *Nat. Struct. Mol. Biol.* **22**, 383-389.

Lynch, C. D., Gauthier, N. C., Biais, N., Lazar, A. M., Roca-Cusachs, P., Yu, C.-H. and Sheetz, M. P. (2011). Filamin depletion blocks endoplasmic spreading and destabilizes force-bearing adhesions. *Mol. Biol. Cell* **22**, 1263-1273.

Masià-Balagué, M., Izquierdo, I., Garrido, G., Cordomí, A., Pérez-Benito, L., Miller, N. L. G., Schlaepfer, D. D., Gigoux, V. and Aragay, A. M. (2015). Gastrin-stimulated Gα13 activation of rgnef protein (ArhGEF28) in DLD-1 colon carcinoma cells. *J. Biol. Chem.* **290**, 15197-15209.

Mayle, K. M., Le, A. M. and Kamei, D. T. (2012). The intracellular trafficking pathway of transferrin. *Biochim. Biophys. Acta* **1820**, 264-281.

Mayor, S., Presley, J. F. and Maxfield, F. R. (1993). Sorting of membrane components from endosomes and subsequent recycling to the cell surface occurs by a bulk flow process. *J. Cell Biol.* **121**, 1257-1269.

Minsaas, L., Planagumà, J., Madziva, M., Krakstad, B. F., Masià-Balagué, M., Katz, A. A. and Aragay, A. M. (2010). Filamin a binds to CCR2B and regulates its internalization. *PLoS ONE* **5**, e12212.

Muriel, O., Echarri, A., Hellriegel, C., Pavón, D. M., Beccari, L. and Del Pozo, M. A. (2011). Phosphorylated filamin A regulates actin-linked caveolae dynamics. *J. Cell Sci.* **124**, 2763-2776.

Nakamura, F., Osborn, T. M., Hartemink, C. A., Hartwig, J. H. and Stossel, T. P. (2007). Structural basis of filamin A functions. *J. Cell Biol.* **179**, 1011-1025.

Nakamura, F., Stossel, T. P. and Hartwig, J. H. (2011). The filamins: organizers of cell structure and function. *Cell Adh. Migr.* **5**, 160-169.

Onoprishvili, I., Andria, M. L., Kramer, H. K., Ancevska-Taneva, N., Hiller, J. M. and Simon, E. J. (2003). Interaction between the opioid receptor and filamin A is involved in receptor regulation and trafficking. *Mol. Pharmacol.* **64**, 1092-1100.

Patel, S., Mukovozov, I. and Robinson, L. A. (2011). Assessment of the recycling of the membrane-bound chemokine, CX_3CL1. *Methods Mol. Biol.* **748**, 143-153.

Planagumà, J., Minsaas, L., Pons, M., Myhren, L., Garrido, G. and Aragay, A. M. (2012). Filamin A-hinge region 1-EGFP: a novel tool for tracking the cellular functions of filamin A in real-time. *PLoS ONE* **7**, e40864.

Popowicz, G. M., Schleicher, M., Noegel, A. A. and Holak, T. A. (2006). Filamins: promiscuous organizers of the cytoskeleton. *Trends Biochem. Sci.* **31**, 411-419.

Puthenveedu, M. A., Lauffer, B., Temkin, P., Vistein, R., Carlton, P., Thorn, K., Taunton, J., Weiner, O. D., Parton, R. G. and Von Zastrow, M. (2010). Sequence-dependent sorting of recycling proteins by actin-stabilized endosomal microdomains. *Cell* **143**, 761-773.

Rabut, G. and Ellenberg J. (2005). Photobleaching techniques to study mobility and molecular dynamics of proteins in live cells: FRAP, iFRAP and FLIP. In *J. In "Live Cell Imaging: A Laboratory Manual* (ed. R.D. Goldman and D. L. Spector), pp. 101-127. Cold Spring Harbor: Cold Spring Harbor Laboratory Press.

Sallusto, F. and Baggiolini, M. (2008). Chemokines and leukocyte traffic. *Nat. Immunol.* **9**, 949-952.

Savoy, R. M. and Ghosh, P. M. (2013). The dual role of filamin A in cancer: can't live with (too much of) it, can't live without it. *Endocr. Relat. Cancer* **20**, R341-R356.

Scott, M. G. H., Pierotti, V., Storez, H., Lindberg, E., Thuret, A., Muntaner, O., Labbé-Jullié, C., Pitcher, J. A. and Marullo, S. (2006). Cooperative regulation of extracellular signal-regulated kinase activation and cell shape change by filamin A and beta-arrestins. *Mol. Cell. Biol.* **26**, 3432-3445.

Seck, T., Baron, R. and Horne, W. C. (2003). Binding of filamin to the C-terminal tail of the calcitonin receptor controls recycling. *J. Biol. Chem.* **278**, 10408-10416.

Shapiro, M. J. and Coughlin, S. R. (1998). Separate signals for agonist-independent and agonist-triggered trafficking of protease-activated receptor 1. *J. Biol. Chem.* **273**, 29009-29014.

Temkin, P., Lauffer, B., Jäger, S., Cimermancic, P., Krogan, N. J. and von Zastrow, M. (2011). SNX27 mediates retromer tubule entry and endosome-to-plasma membrane trafficking of signalling receptors. *Nat. Cell Biol.* **13**, 715-721.

Terada, K., Horinouchi, T., Fujioka, Y., Higashi, T., Nepal, P., Horiguchi, M., Karki, S., Hatate, C., Hoshi, A., Harada, T. et al. (2014). Agonist-promoted ubiquitination differentially regulates receptor trafficking of endothelin type A and type B receptors. *J. Biol. Chem.* **289**, 35283-35295.

Tigges, U., Koch, B., Wissing, J., Jockusch, B. M. and Ziegler, W. H. (2003). The F-actin cross-linking and focal adhesion protein filamin a is a ligand and in vivo substrate for protein kinase C. *J. Biol. Chem.* **278**, 23561-23569.

Tirupula, K. C., Ithychanda, S. S., Mohan, M. L., Naga Prasad, S. V., Qin, J. and Karnik, S. S. (2015). G protein-coupled receptors directly bind filamin A with high affinity and promote filamin phosphorylation. *Biochemistry* **54**, 6673-6683.

Travis, M. A., van der Flier, A., Kammerer, R. A., Mould, A. P., Sonnenberg, A. and Humphries, M. J. (2004). Interaction of filamin A with the integrin beta 7 cytoplasmic domain: role of alternative splicing and phosphorylation. *FEBS Lett.* **569**, 185-190.

Yu, N., Erb, L., Shivaji, R., Weisman, G. A. and Seye, C. I. (2008). Binding of the P2Y2 nucleotide receptor to filamin A regulates migration of vascular smooth muscle cells. *Circ. Res.* **102**, 581-588.

Zhang, J., Neal, J., Lian, G., Shi, B., Ferland, R. J. and Sheen, V. (2012). Brefeldin A-inhibited guanine exchange factor 2 regulates filamin A phosphorylation and neuronal migration. *J. Neurosci.* **32**, 12619-12629.